



HAL
open science

Intrinsic Nucleic Acid Dynamics Modulates HIV-1 Nucleocapsid Protein Binding to Its Targets

Ali Bazzi, Loussiné Zargarian, Françoise Chaminade, Hugues de Rocquigny,
Brigitte René, Yves Mély, Philippe Fossé, Olivier Mauffret

► **To cite this version:**

Ali Bazzi, Loussiné Zargarian, Françoise Chaminade, Hugues de Rocquigny, Brigitte René, et al..
Intrinsic Nucleic Acid Dynamics Modulates HIV-1 Nucleocapsid Protein Binding to Its Targets. PLoS
ONE, 2012, 7, pp.e38905. 10.1371/journal.pone.0038905 . hal-03327347

HAL Id: hal-03327347

<https://hal.science/hal-03327347>

Submitted on 27 Aug 2021

HAL is a multi-disciplinary open access archive for the deposit and dissemination of scientific research documents, whether they are published or not. The documents may come from teaching and research institutions in France or abroad, or from public or private research centers.

L'archive ouverte pluridisciplinaire **HAL**, est destinée au dépôt et à la diffusion de documents scientifiques de niveau recherche, publiés ou non, émanant des établissements d'enseignement et de recherche français ou étrangers, des laboratoires publics ou privés.

Intrinsic Nucleic Acid Dynamics Modulates HIV-1 Nucleocapsid Protein Binding to Its Targets

Ali Bazzi¹, Loussiné Zargarian¹, Françoise Chaminade¹, Hugues De Rocquigny², Brigitte René¹, Yves Mély², Philippe Fossé¹, Olivier Mauffret^{1*}

1 Laboratoire de Biologie et Pharmacologie Appliquée, Ecole Normale Supérieure de Cachan, Centre National de la Recherche Scientifique, Cachan, France, **2** Laboratoire de Biophotonique et Pharmacologie, Centre National de la Recherche Scientifique Unité mixte de Recherche 7213, Faculté de Pharmacie, Université de Strasbourg, Illkirch, France

Abstract

HIV-1 nucleocapsid protein (NC) is involved in the rearrangement of nucleic acids occurring in key steps of reverse transcription. The protein, through its two zinc fingers, interacts preferentially with unpaired guanines in single-stranded sequences. In mini-cTAR stem-loop, which corresponds to the top half of the cDNA copy of the transactivation response element of the HIV-1 genome, NC was found to exhibit a clear preference for the TGG sequence at the bottom of mini-cTAR stem. To further understand how this site was selected among several potential binding sites containing unpaired guanines, we probed the intrinsic dynamics of mini-cTAR using ¹³C relaxation measurements. Results of spin relaxation time measurements have been analyzed using the model-free formalism and completed by dispersion relaxation measurements. Our data indicate that the preferentially recognized guanine in the lower part of the stem is exempt of conformational exchange and highly mobile. In contrast, the unrecognized unpaired guanines of mini-cTAR are involved in conformational exchange, probably related to transient base-pairs. These findings support the notion that NC preferentially recognizes unpaired guanines exhibiting a high degree of mobility. The ability of NC to discriminate between close sequences through their dynamic properties contributes to understanding how NC recognizes specific sites within the HIV genome.

Citation: Bazzi A, Zargarian L, Chaminade F, De Rocquigny H, René B, et al. (2012) Intrinsic Nucleic Acid Dynamics Modulates HIV-1 Nucleocapsid Protein Binding to Its Targets. PLoS ONE 7(6): e38905. doi:10.1371/journal.pone.0038905

Editor: Claudine Mayer, Institut Pasteur, France

Received: February 27, 2012; **Accepted:** May 14, 2012; **Published:** June 20, 2012

Copyright: © 2012 Bazzi et al. This is an open-access article distributed under the terms of the Creative Commons Attribution License, which permits unrestricted use, distribution, and reproduction in any medium, provided the original author and source are credited.

Funding: This work was supported by Agence Nationale de Recherche sur le Sida (to P.F., O.M. and A.B.) and by Agence Nationale de la Recherche (ANR) project "FemtoSTACK" (to YM). Funding for open access charge came from Centre National de la Recherche Scientifique (CNRS LBPA UMR 8113). The funders had no role in study design, data collection and analysis, decision to publish, or preparation of the manuscript.

Competing Interests: The authors have declared that no competing interests exist.

* E-mail: olivier.mauffret@bpa.ens-cachan.fr

Introduction

The human immunodeficiency virus type 1 (HIV-1) nucleocapsid protein (NC) is a small (55 amino acids) basic protein characterized by two zinc fingers and a basic N-terminal domain [1,2]. NC exhibits numerous functions all along the virus replication cycle [2–8], being notably involved in selective packaging of unspliced viral genomic RNA and chaperoning of nucleic acid strands during reverse transcription. The multiple roles of NC in virus replication are thought to result from its interplay with various target nucleic acid sequences [1]. At high concentrations, NC can bind non specifically to any DNA and RNA sequence of 5–7 nt length. In contrast, at low concentrations, the binding of NC strongly depends on the sequence and the structure of the DNA or RNA sequence [2,9–11]. Numerous *in vitro* studies support the notion that NC zinc fingers are responsible for specific interactions, whereas the basic N-terminal domain is involved in non-specific binding [1,2,12–16]. A clear-cut feature of NC is its preference for single-stranded regions (bulges, loops, linear fragments,...) over double-stranded sequences and its ability to destabilize short double-strand regions. Interestingly, NC exhibits higher affinity for sequences containing unpaired guanines [2,11]. More precisely, sequences containing TG, UG, and GNG (where N corresponds to either A, C, T or U) motifs are preferred [9–11,17,18]. High-resolution structures allow understanding the

structural basis for this specificity, by showing that insertion of an unpaired guanine into the hydrophobic platform at the top of the folded zinc fingers is systematically present in all solved complexes. This insertion is thought to be critical for discriminating the guanine residue from the other bases [9,11,19–21].

In this context, one important question is to understand the molecular basis of the selective binding of NC to particular sequences, such as for instance the SL2 and SL3 stem-loops involved in the specific packaging of the unspliced viral RNA genome [11,22]. The recent determination of the architecture and secondary structure of the entire HIV-1 RNA genome [23] indicates that large portions are double-stranded, suggesting that NC specific sites are limited. Furthermore, data with the Gag protein and the MuLV retroviral genome [24] indicate that the local context can considerably increase the NC affinity for particular sequences and show that a short motif (4 nt) with a low information content can be discriminated and identified in the entire viral genome. However, understanding of the molecular mechanisms involved in the selection process is limited and requires additional studies.

Using NMR methods, we recently investigated the binding of NC(11–55) to mini-cTAR, a model stem-loop DNA molecule of 26 nt [20,25], that corresponds to the top half of cTAR, the complementary sequence of TAR (Trans activating response

element) RNA [6,14,15,26–28]. The annealing of cTAR with TAR is necessary for the first strand transfer of reverse transcription [6,29]. The determination of the three-dimensional structure of mini-cTAR:NC(11–55) complex allowed by comparison with other reported NC:nucleic acid structures to identify the molecular determinants of the opposite binding polarity of NC on DNA molecules as compared to RNA molecules [20]. Interestingly, although five guanines of mini-cTAR are not involved in stable base pairing (defined on the basis of the presence or absence of a detectable imino proton signal at 10°C) in free cTAR and constitutes therefore potential binding sites, our NMR data indicate only one major binding site in mini-cTAR corresponding to the G26 residue of the ²⁴TGG²⁶ sequence at the 3′-end [20,25]. Furthermore, all nucleic acid partners of NC used in the previous NMR studies had only one NC binding site [9,11,19,21] and only in one case a minor binding site was identified besides the main site [19]. Therefore, the nearly exclusive binding of NC to the TGG sequence at the 3′-end of mini-cTAR is intriguing as is also the absence of significant binding to the apical and internal loops that contain unpaired guanines.

To further understand the origin of the preferential recognition of the TGG sequence by NC and the absence of significant binding in apical and internal loops, quantitative information on the motions experienced by DNA molecules in the presence and absence of NC are needed to complete the previous structural studies and to provide insights into the role of dynamics in the NC:DNA recognition. Although the top half of TAR RNA has been the subject of numerous NMR studies that describe the internal dynamics and relative motions of the stems of this hairpin [30–35], the cTAR element has been little studied with NMR methods. Here, using ¹³C spin relaxation, and relaxation dispersion measurements [35–39], we quantified the mini-cTAR DNA dynamics. Quantitative analysis of the relaxation data identified the main sites of the fast dynamical processes (in the ps-ns timescale) as well as the slow motions (in the μs-ms time scale). The relaxation rates and heteronuclear NOE have been measured for the C6, C8 and C1′ sites which allowed depicting the dynamics of residues at the level of both the bases and deoxyribose sugars. Large differences in the dynamics between the various parts of the hairpin were observed. Moreover, we identified several putative transient base pairs in the apical and internal loops and investigated their role in the stability of the different parts of the hairpin. Interestingly, due to these transient base pairs the unpaired guanines in the apical and internal loops and the lower stem are not fully accessible to interact optimally with NC. Therefore, only the guanines of the TGG sequence being not involved in transient base-pairs can constitute a strong binding site in this model sequence.

Materials and Methods

DNA Preparation

Uniformly ¹⁵N-¹³C enriched mini-cTAR DNA stem loop (26 nt) was obtained from SILANTES. For NMR studies, the labeled mini-cTAR (26) was dissolved in 300 μl (shigemi tube) of 13 mM Na/Na₂(PO₄) buffer (pH 6.5), 30 mM NaCl, and 0.2 mM MgCl₂. After lyophilization, labeled mini-cTAR was dissolved in D₂O. The final sample concentration of mini-cTAR was 0.75 mM. NC(11–55) was synthesized by the stepwise solid phase method with Fmoc amino acids as described [40] and its purity was greater than 98%. NC(11–55) was prepared with 3 equivalents of ZnCl₂ to ensure saturation of the finger motifs.

Gel Retardation Assays

Mini-cTAR DNA was 5′-end labeled using T4 polynucleotide kinase (New England Biolabs, Ipswich, MA) and [γ -³²P] ATP (Perkin Elmer, Waltham, MA). The 5′-end labeled mini-cTAR was purified by electrophoresis on a 15% denaturing polyacrylamide gel and isolated by elution followed by ethanol precipitation. Assays were carried out in a final volume of 10 μl. Mini-cTAR ³²P-DNA (10 pmol) at 2 × 10³ cpm/pmol was dissolved in 6 μl of water, heated at 90°C for 2 min and chilled for 2 min on ice. Then, 2 μl of renaturation buffer was added (final concentrations: 30 mM NaCl, 0.2 mM MgCl₂ and 25 mM Tris-HCl pH 7.5) and the sample was incubated for 15 min at 20°C in the absence or presence of protein at various concentrations. Gel loading buffer (final concentrations: 10% w/v glycerol, 0.01% w/v bromophenol blue, 0.01% w/v xylene cyanol) was added and the samples were analyzed by electrophoresis on a 14% polyacrylamide gel (Acrylamide:Bis-acrylamide = 29:1) at 4°C in 0.5 × TBE buffer (45 mM Tris-borate pH 8.3, 1 mM EDTA). After electrophoresis, the gel was fixed, dried and autoradiographed. Free DNA and protein:DNA complexes were quantified using a Molecular Dynamics Typhoon imager and ImageQuant software (Molecular Dynamics, GE Healthcare Bio-Sciences Corp., Piscataway, NJ). The fraction of bound mini-cTAR DNA (FR) was determined using the formula $FR = 1 - \left(\frac{IF}{IB + IF} \right)$, where IF and IB are the band intensities of free and bound mini-cTAR DNAs, respectively.

NMR Relaxation Experiments

All NMR experiments were recorded at 298 K on Bruker Avance-500 spectrometer. Data were collected on BBI probes. Longitudinal relaxation rates (R_1), transverse relaxation rates in the rotating frame ($R_{1\rho}$) and heteronuclear NOE measurements were carried out for C8, C6 and C1′ carbons and were recorded as a series of 2D NMR spectra, in which the relaxation delay τ was parametrically increased. $R_{1\rho}$ experiments were executed at a spin-lock field of 2 kHz with the carrier positioned at the center of the ¹³C resonance region. Since the different pairs of scalar coupled carbons resonate in distinct spectral regions, $R_{1\rho}$ can be measured for C6 and C1′ without interference from unwanted magnetization transfers. Nonzero offsets of individual resonances cause measured $R_{1\rho}$ values to have contributions from R_1 in addition to $R_{1\rho}$. The true $R_{1\rho}$ values were extracted according to: $R_{1\rho}(\text{measured}) = R_1 \cos^2 \beta + R_{1\rho} \sin^2 \beta$ in which $\beta = \arctan \left(\frac{v_{SL}}{\Omega} \right)$ is the effective tilt angle of the spin-lock field, with v_{SL} and Ω being the spin-lock field strength and resonance offset in Hz respectively [38,39]. The relaxation delay between scans was set to 2 s. The ¹³C carrier frequency was set to the center of the carbon resonance region of interest for the aromatic carbons and for the C1′. The ¹³C-¹H correlation experiments were carried out with 86 × 2048 points with 48 scans for relaxation rate measurements on C6 and C8 carbons, whereas 120 × 2048 points were used for C1′ carbon with 48 scans.

Selective excitation was accomplished by application of ¹³C 180° IBURP1-shaped pulses during the first INEPT transfer to allow selective excitation of the described carbon resonances [41]. In addition, the ¹³C frequency labeling was implemented with a constant-time evolution period set to n/J_{CC} where J_{CC} is the scalar coupling between directly bonded carbons. The constant time delays were set to 7.10 and 12.5 ms when base and sugar relaxation properties were recorded, respectively, corresponding to ¹³C-¹³C coupling constants of approximately 70 Hz (bases) and 40 Hz (sugars). Delays of 5 ms, 20 ms, 60 ms, 100 ms, 200 ms,

400 ms, 700 ms, and 1000 ms; 4 ms, 8 ms, 12 ms, 24 ms, 32 ms, 48 ms, 64 ms, and 96 ms; 5 ms, 20 ms, 60 ms, 100 ms, 200 ms, 400 ms, 700 ms, 1000 ms respectively, were used for T_1 and $T_{1\rho}$ experiments of base ^{13}C (C8 and C6) resonances. Several experimental points were repeated three times to evaluate the reproducibility of the measurements (60 ms, 200 ms and 700 ms for T_1 , 12 ms, 32 ms and 48 ms for $T_{1\rho}$ C8, and 60 ms, 200 ms, and 700 ms for $T_{1\rho}$ C6). Delays of 5 ms, 20 ms, 60 ms, 100 ms, 200 ms, 400 ms, 700 ms, 1000 ms, and 4 ms, 8 ms, 12 ms, 24 ms, 32 ms, 48 ms, 64 ms, 94 ms respectively, were used for T_1 and $T_{1\rho}$ of sugar (C1') ^{13}C resonances. Two times points in $T_{1\rho}$ were repeated (12 ms and 48 ms). Relaxation rates and errors due to uncertainty in experimental measurements were determined by fitting the intensity to a monoexponential decay using GraphPad Prism software. For heteronuclear NOE (hetNOE) measurements, a pair of spectra were recorded, one with initial proton saturation and one without. Spectra recorded with proton saturation utilized a relaxation delay of 2.5 s followed by a 2.5 s period of saturation. Spectra recorded in the absence of saturation employed a recycle delay of 2.5 s. Heteronuclear NOE spectra were collected at 500 MHz for the C6, C8 and C1' resonances.

Data reporting on the power dependence of $T_{1\rho}$ were collected and analyzed for C8, C6 and C1' resonances. A series of $T_{1\rho}$ experiments at various spin-lock field strengths was collected (0.9 kHz, 1.7 kHz, 2.6 kHz, 3.7 kHz, 5.2 kHz and 6.5 kHz). These values were set by modifying the power level of the spin-lock pulse. Data at each power level were collected and analyzed independently with the same settings and delays as those described above for $T_{1\rho}$ data collection. Delays of 4 ms, 8 ms, 12 ms, 16 ms, 24 ms, 32 ms, and 48 ms were used for $T_{1\rho}$ experiments for base ^{13}C resonances. For sugars, delays of 12 ms, 20 ms, 28 ms, 40 ms, 60 ms and 80 ms were used. However, for the higher spin-lock fields (3.7 kHz, 5.2 kHz and 6.5 kHz), the longest relaxation delay was set to 28 ms to avoid sample heating, and delays were set to 4 ms, 8 ms, 12 ms, 16 ms, 24 ms, 28 ms for bases and 4 ms, 8 ms, 12 ms, 16 ms, 24 ms, 28 ms for sugars C1'.

Data Analysis

Values of T_1 and $T_{1\rho}$ were determined by fitting the measured peak volumes for each assigned peak into an exponential decay. Briefly, T_1 and $T_{1\rho}$ values were determined from the decay curves using the standard equation:

$$I(\tau) = I_0 \exp(-\tau/T_1) \tag{1}$$

where I_0 is the initial peak intensity and τ is the delay time. The errors (S.D.) were estimated by the GraphPad Prism software. The hetNOE values were calculated from the ratio of the intensity of saturated/unsaturated spectra. Standard C-H bond lengths have been employed in all calculations. Commonly used C-H bond lengths are 1.08 Å for C6–H6/C8–H8 and 1.09 Å for C1'–H1', respectively [42]. We used the values of chemical shift anisotropies (CSA) recently reported for C6/C8 (adenine 144 ppm, cytosine 186 ppm, guanine 133 ppm and thymine 168 ppm) [43,44] while 30 ppm have been used for C1' sugar [44,45].

Analysis of Relaxation Data with ModelFree

The model-free analysis of the relaxation parameters has been carried out using the ModelFree 4.0 program by Palmer and co-workers [46]. ModelFree parameters were fit to one of the five models, where the following parameters are varied: (1) S^2 , (2) S^2 and an effective internal correlation time for fast motions τ_e , (3) S^2 and transverse relaxation exchange parameter R_{ex} , (4) S^2 , τ_e and

R_{ex} , and (5) the order parameters for shorter and longer timescale motion (S^2_f , S^2_{ss} , τ_f , τ_s).

For C6 and C8 carbon atoms, three residues (T10, C23 and T24) could be fit with model 2, two residues (G4, G8) were fit with model 3, five residues (C1, A5, C11, C12 and C22) with model 4 and the 11 remaining residues with model 1. For the anomeric resonances, four residues (G6, C9, T18 and C19) could be fit with model 1; three residues (A5, A7 and G20) could be fit with model 4. No residues were fit with model 3 and model 5. Residues C2, G4, T10, G14, A21, T24, G25 and G26 could not be fit with any model. C11 and C22 resonances overlapped. The nine remaining residues were fit with model 2.

Results

Analysis of the Sequence-specific Binding of NC to Mini-cTAR

The NC binding to mini-cTAR has been reported in our precedent NMR study [20]. We showed that the binding is almost restricted to a single site: the TGG sequence located at the 3'-end of the lower stem which alternates between single-stranded and double-stranded states [25], as a consequence of the destabilization induced by the internal loop. To gain further insight into the mini-cTAR DNA recognition by NC, we first carried out gel retardation assays with NC(11–55) (a truncated form of NC) and wild-type and mutant mini-cTAR DNAs (Figures 1 and 2). Interestingly, comparison with heat-denatured mini-cTAR DNAs (Figure 2A, lanes 2) revealed that the various mini-cTAR derivatives remained monomeric after renaturation and incubation with NC(11–55) at a protein to nucleotide molar ratio of 1:1 and removal of the protein before gel electrophoresis (Figure 2A, lanes 1). Addition of increasing amounts of NC(11–55) to native mini-cTAR resulted in the appearance of band CI, consistent with the 1:1 NC(11–55):mini-cTAR complex evidenced by NMR (Figure 2A). The IN2 mutant was designed so that the internal loop was deleted and the TGG sequence was predicted to be located in a stable double-stranded stem. Protein:DNA complexes were barely detectable with this mutant (Figure 2A and B), showing that NC(11–55) did not interact tightly with the apical loop of IN2, despite the presence of two unpaired guanines. The CT mutant was designed so that a single point mutation created a TGG sequence in the apical loop. Addition of increasing amounts of NC(11–55) resulted in the appearance of bands CI and CII, suggesting that the CT mutant contained two binding sites for the peptide: the TGG sequence at the 3'-end and the TGG sequence in the apical loop. The IN2CT mutant was designed so that the hairpin contained only one potential NC binding site corresponding to the unpaired TGG sequence in the apical loop. As expected, NC(11–55) bound mini-cTARIN2CT tightly with a 1:1 stoichiometry, but the amount of protein:DNA complexes was less than with the wild-type (Figure 2B), indicating that the NC(11–55) binding strength depends on whether the TGG sequence is located at the 3'-end or in the apical loop. Therefore, the context of the unpaired TGG sequence appears important for NC(11–55) binding.

Taken together, one of the most intriguing features in our data was the poor binding ability of the CGG sequence in the apical loop of mini-cTAR. This may result from poor accessibility and availability of guanines, as a consequence of their dynamics in this context. To check this hypothesis, NMR ^{13}C relaxation measurements were performed to probe the dynamic properties of the various residues of mini-cTAR with a particular focus on guanines.

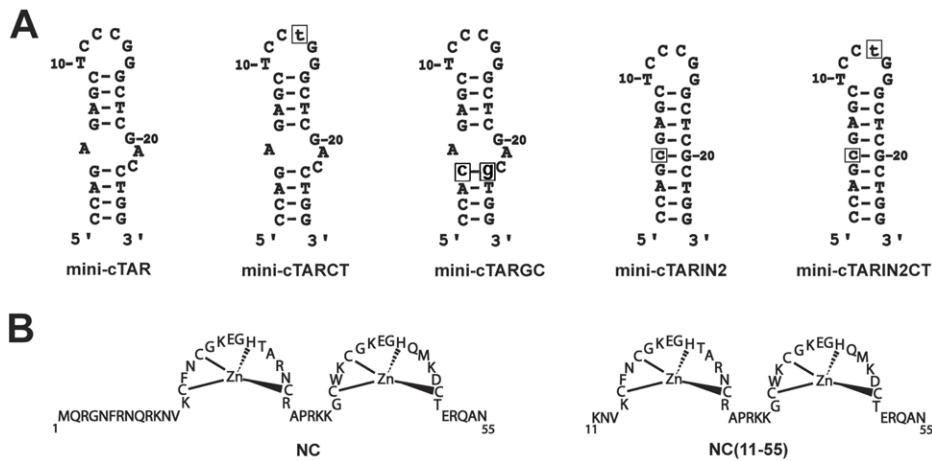


Figure 1. DNA oligonucleotides and peptides used in the study (A) Secondary structures for the mini-cTAR sequences. The single base mutations are boxed. (B) Sequences of NC and NC(11–55). doi:10.1371/journal.pone.0038905.g001

Data Collection and Qualitative Analysis

To probe the dynamic properties of the mini-cTAR molecule, we recorded the ^{13}C relaxation parameters of aromatic (C6, C8) and anomeric (C1') carbons. Proton and carbon (C6, C8, C1') resonance assignments for the mini-cTAR DNA residues were available from our previous study [25]. The ^{13}C relaxation rates of C6, C8 and C1' carbons were measured using a ^{13}C , ^{15}N -labeled sample of mini-cTAR. ^{13}C , T_1 , $T_{1\rho}$ and hetNOEs were recorded for the aromatic and C1' carbons using the constant time version of the pulse sequences modified for application to nucleic acids [41,47,48] as described in Materials and Methods. Typical T_1 and $T_{1\rho}$ relaxation decay curves are presented in Figure S1. Measured relaxation times T_1 , $T_{1\rho}$, ^1H - ^{13}C hetNOEs are shown in Figure 3 for C6 and C8 carbons, and in Figure S2 for C1' carbons. To simplify the analysis, the mini-cTAR molecule was divided in four regions corresponding to the upper stem, lower stem, apical loop and internal loop (Figure 3). To compare the global properties of each part, we determined the average values for T_1 , $T_{1\rho}$ and hetNOE values for purine, pyrimidine bases and C1' carbons for each part of the molecule (Table 1). Since only the upper stem is fully double-stranded [25], its values provided reference points to evaluate the relaxation properties of the other regions. For the upper stem, the relaxation parameters are ordered according to the following hierarchy: $T_{1-C1'}$ (470 ms) $>$ $T_{1-purines}$ (437 ms) $>$ $T_{1-pyrimidines}$ (360 ms); $T_{1\rho-C1'}$ (44 ms) $>$ $T_{1\rho-purines}$ (35 ms) $>$ $T_{1\rho-pyrimidines}$ (33 ms); hetNOE $_{-C1'}$ (1.35) $>$ hetNOE $_{-purines}$ (1.23) $>$ hetNOE $_{-pyrimidines}$ (1.13). Interestingly, the hierarchy and the mean values are similar to those obtained for a DNA duplex [44] and for double-stranded regions in an RNA stem-loop [47], recorded at a similar frequency of 500 MHz. The relaxation differences between the three carbon classes (C8, C6 and C1') are known to be related to large differences in chemical shift anisotropies between these three classes [47,49–51].

Relative to the upper stem, lower values for T_1 and higher values for $T_{1\rho}$ and hetNOE were observed for most residues of the apical loop and the lower stem (Table 1 and Comments on Figure 3 and Figure S2); suggesting the presence of fast motions on the picosecond to nanosecond time scale in these two parts of mini-cTAR [47,52]. The average values for the internal loop do not show similar behavior, suggesting limited motions for this loop in the same time scale. Altogether, these data are consistent with

our previous structural study indicating that, globally, residues of the apical loop and of the lower stem are poorly structured [25].

Quantitative Analysis of the ^{13}C Relaxation Data

Besides the qualitative features exposed above, the data were analyzed to get further information about the global motion, fast internal motions and slow conformational fluctuations of mini-cTAR. The procedure has been described extensively in previous works [41,46,53] and additional details are furnished as Materials S1 that were fitted with both axially symmetric and isotropic diffusion models and few differences were found between the residuals of the fits of the two models. The value for the global correlation time (5.1 ns) is close to that obtained for RNA molecules of similar size [47,51]. The value of diffusion anisotropy ($D_{\parallel}/D_{\perp} = 1.15$) is slightly higher than 1 and indicates that the mini-cTAR structure did not present an elongated form [47]. This is in line with previous findings indicating that only the upper stem is stably formed, resulting probably in a non-elongated shape for mini-cTAR [25]. In contrast, the structure of the top half of the TAR RNA hairpin has been shown to be highly anisotropic with a $D_{\parallel}/D_{\perp} = 2.0$ [54], consistent with the presence of two stems; each stem being composed of 4–6 base-pairs and separated by a three-base bulge. Another case that could be compared with the present data is the 23-nucleotide SRE, an RNA hairpin containing a long stem of 9 base-pairs, and for which a D_{\parallel}/D_{\perp} value of 1.49, indicating a significant degree of anisotropy, has been measured [51].

Internal Motions

To extract information on the internal motions of individual residues, the relaxation data (RI , $RI\rho$, hetNOEs) were analyzed for the residues for which a complete set of measurements can be made. The relaxation data were analyzed with five models of different complexities: (1) S^2 ; (2) S^2 , τ_e ; (3) S^2 , R_{ex} ; (4) S^2 , τ_e , R_{ex} ; (5) S^2 f, S^2 , τ_e using the model-free program [46,55] to select the best model for each residue [42,46,47,51,54]. Several issues are known to complicate the analysis of ^{13}C relaxation data for nucleic acids, such as the asymmetry of the chemical shift anisotropies, the non-collinearity of these latter with the C-H dipolar tensor, and the contribution to ^{13}C relaxation from dipolar interaction with adjacent ^{13}C and ^{15}N spins [42,47,49–51,54]. In the present case, these effects are expected to be weak considering the nearly

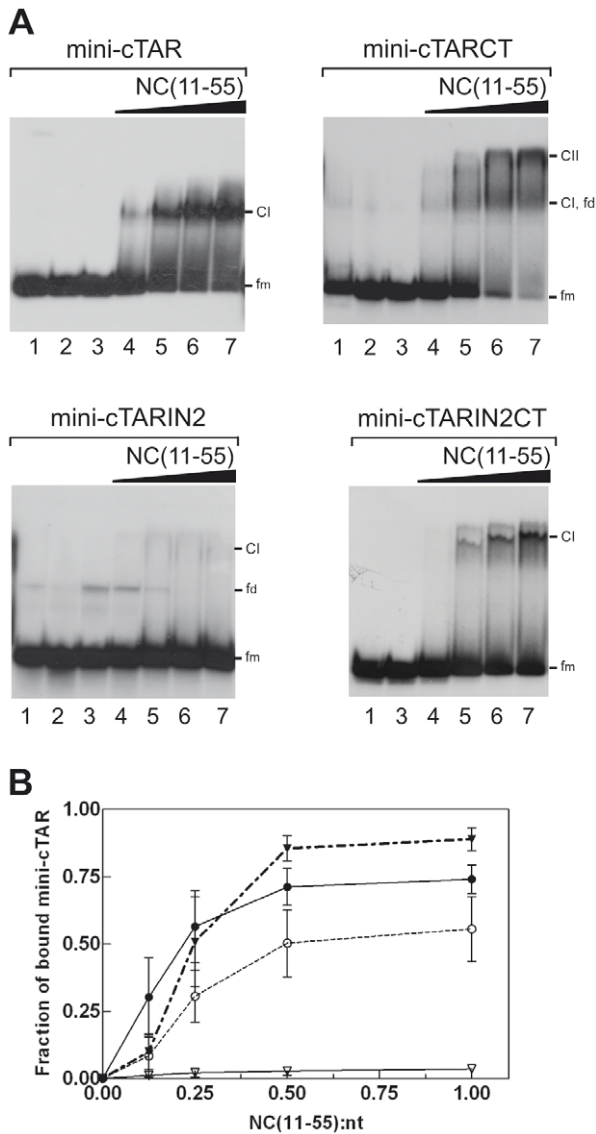


Figure 2. Gel retardation assays of NC(11–55):mini-cTAR DNA complexes formed *in vitro*. (A) Mini-cTAR 32 P-DNAs were incubated in presence of NC(11–55) and analyzed by electrophoresis on a 14% polyacrylamide gel as described in Materials and Methods. Lanes 1, controls mini-cTAR dimerization induced by NC(11–55) at a protein to nucleotide molar ratio of 1:1 (NC(11–55) was removed by phenol/chloroform before gel electrophoresis); lanes 2, heat-denatured mini-cTAR DNAs; lanes 3, controls without protein; lanes 4–7, protein to nucleotide molar ratios were 1:8, 1:4, 1:2 and 1:1. Monomeric and dimeric forms of free mini-cTAR DNAs are indicated by fm and fd, respectively. Cl and CII indicate the NC(11–55):mini-cTAR complexes. (B) Fraction of bound mini-cTAR as a function of the protein:oligonucleotide (expressed in nt) ratio. Each data point represents the mean of three experiments. Symbols: filled circles, mini-cTAR; filled triangles, mini-cTARCT; open triangles, mini-cTARIN2; open circles, mini-cTARIN2CT.

doi:10.1371/journal.pone.0038905.g002

isotropic behavior of cTAR, its small correlation time and the relatively average field (500 MHz) used for the study [47,54].

Results obtained for the different analyzed spins are reported in Table 2. For the aromatic carbons, most (7 out of 8) of the residues of the upper stem (G6–C9 and G16–C19) could be described by the most simple model (only the S^2 parameter and internal fast

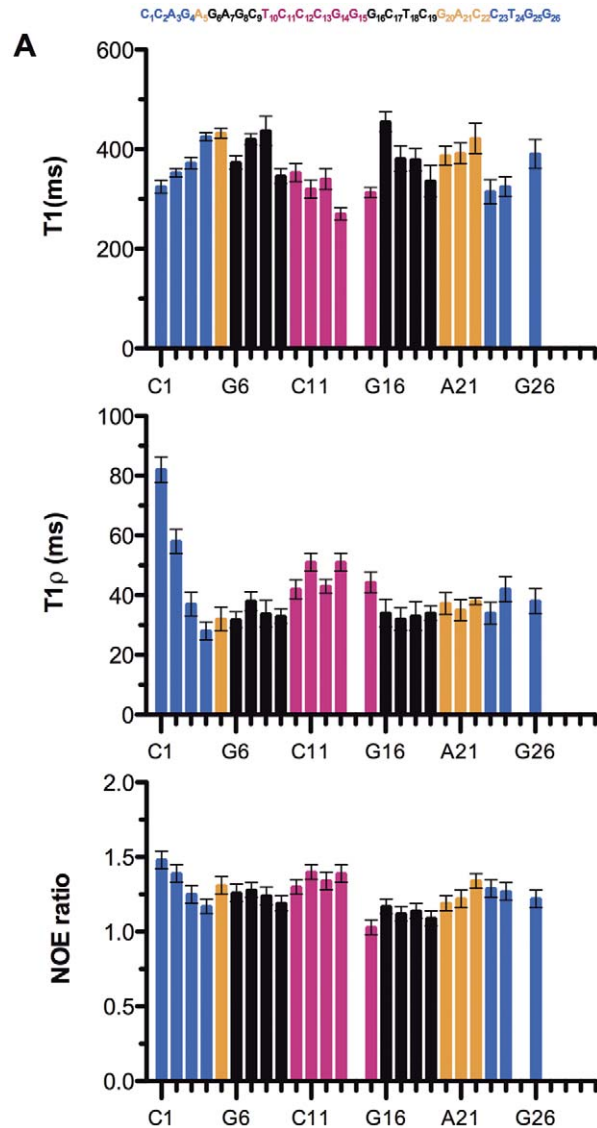


Figure 3. Relaxation times for aromatic C6/C8 spins of mini-cTAR DNA at 500 MHz. Top to bottom: ^{13}C T_1 , ^{13}C $T_{1\rho}$ and hetNOEs. Errors represent uncertainties in the fit of the primary relaxation data to mono-exponential decays. No data are associated to residues corresponding to a broad or overlapped cross peak. The color codes used for the residues are the following: blue (lower stem), orange (internal loop), black (upper stem) and magenta (apical loop). doi:10.1371/journal.pone.0038905.g003

time motions less than 20 ps) [46]. In contrast, the residues of the apical loop (T10–G15) are described by models 2 and 4 with correlation times for the internal motions in the range 15–100 ps. The internal motions of the internal loop residues G20 and A21 could be described by model 1 but more complex models were needed for A5 and C22 residues with correlation time in the range 40–65 ps and significant exchange contributions (R_{ex}). Complex model are also necessary to describe the terminal C1, C23 and T24 residues of the lower stem. The S^2 values are reported in Figure 4 (S^2 ranges are between 0 (unrestricted motion) and 1 (highly restricted motion)). The upper stem residues (Figure 4A) show restricted motion (S^2 in the range 0.88–1) consistent with the double-strand character of this part of mini-cTAR [25]. Lower S^2 values (S^2 in the range 0.67–0.81) indicative of less restricted motions are found for the pyrimidine residues of the apical loop

Table 1. Average Relaxation times T_1 , $T_{1\rho}$ and NOE ratios for base and sugar resonances for each domain of mini-cTAR DNA.

	T_1 (ms)	$T_{1\rho}$ (ms)	NOE ratio
Upper stem			
C8-H8	437	35	1.23
C6-H6	360	33	1.13
C1'-H1'	470	44	1.35
Lower stem			
C8-H8	396	34	1.21
C6-H6	329	54	1.35
C1'-H1'	446	49	1.54
Internal loop			
C8-H8	403	34	1.24
C6-H6	421	38	1.34
C1'-H1'	471	37	1.36
Apical loop			
C8-H8	313	44	1.03
C6-H6	320	47	1.35
C1'-H1'	428	44	1.48

doi:10.1371/journal.pone.0038905.t001

(Figure 4A), consistent with the weak stacking interactions of these residues in the structure [25]. For the anomeric carbons, the differences in S^2 are less significant between the residues of the different parts of the molecule, but the trends are similar (Table 2 and Figure 4B) since for instance the C12, C13 and G20 residues of the apical and internal loops exhibit lower S^2 values than the residues of the upper stem (0.8–1.0). The residues of the lower stem were more difficult to fit since no model could describe the relaxation data of T24, G25, and G26. Finally, while ^1H - ^{13}C aromatic cross-peaks of G25 and G26 overlap partially, ^1H - ^{13}C anomeric cross peaks for these two residues are clearly separated and intensities could be measured. Interestingly, while we could not fit the data of G25 and G26 to one of the models, the $T_{1\rho}$ and hetNOE values are higher for G26 than for G25 (Figure S2), suggesting higher mobility for G26. The large differences in the internal motions of residues from the different parts of the molecule are in full agreement with the data from our structural study [25].

Slow Conformational Exchange Fluctuations

The presence of slow motions in the μs -ms range led to an increase in the transverse relaxation rate by a factor R_{ex} [39,46,56]. As a consequence, resonances exhibiting slow motions show a decrease in $R_{1\rho}$ as the power of the spin-lock field is increased. This power dependence of $R_{1\rho}$ for the aromatic and anomeric carbons of several residues is shown in Figure 5 and the R_{ex} values that could be deduced from these curves are shown in Figure 6 for the aromatic carbons. The residues A5, G20 and C22 of the internal loop and the adjacent G4 residue present large slow exchange contributions. In contrast, in the upper stem and the apical loop, small exchange contributions are observed, with the exception of residue C11. Residues C1–A3 and T24–G26 of the lower stem present medium R_{ex} values. The model-free analysis described in the preceding section can also be used to extract R_{ex} values independently from the dispersion relaxation experiments.

Comparison of the data with the two methods establishes that G4, A5 and C22 exhibit the largest R_{ex} values (Table 2).

The data from anomeric carbons confirm the large exchange contributions for residues G4, A5, G20 and C22. Using both dispersion relaxation experiments and model-free analysis, we observe that the residues in the double-stranded part of mini-cTAR are devoid of significant exchange contributions and constitute therefore excellent controls for the reliability of the experiments. In the case of the C8 carbon of G14 residue, the corresponding cross-peaks are so broadened that it is not possible to reliably measure its intensity (it is the lowest intensity cross-peak in Figure S3). Such behavior is typical of large R_{ex} contribution and slow exchange conformational fluctuations that are well known to impact directly the line width. Although the relaxation parameters could not be measured for the aromatic carbon of residue G14, it was possible to deduce from the recorded spectra that this residue possesses a large R_{ex} value.

Taken together, the dispersion relaxation experiments, model-free analysis and qualitative observation of line broadenings demonstrate that four residues of the internal loop (A5, G20, A21 and C22), two residues of apical loop (C11 and G14) and the adjacent residues of the lower stem (G4, C23) exhibit slow conformational exchange fluctuations. In contrast, no residue of the upper stem is affected by these exchange contributions, demonstrating that the internal loop destabilizes only the lower stem but not the upper stem.

Impact of Mutations in the Lower Stem

To investigate the role of the junction between the internal loop and the lower stem on the stability of mini-cTAR, residues G4 and C23 were permuted in the mini-cTARGC mutant (Figure 1A). Interestingly, additional resonances, relative to mini-cTAR, were observed in the imino proton region (Figure 7). The procedure assignment based on the observation of NOE connectivities designate the new imino protons as those of residues G23 (broadened but clearly observable at 12.4 ppm), T24 and G25. The signal at 11.1 ppm in the two molecules has been assigned to the T10/G15 imino proton (Figure 7A and B). This latter assignment derived from the comparative analysis of a mutant of mini-cTAR in which residue G15 has been replaced by residue A15. The spectra of this mutant showed an additional T imino proton in the Watson-Crick region, as expected from the formation of the new T10–A15 base-pair and concomitantly the disappearance of the imino proton at 11.1 ppm (data not shown). In summary, the observation of three new imino protons in mini-cTARGC demonstrates that the permutation of the G4 and C23 bases strongly stabilizes the lower stem.

Discussion

In this study, we investigated the motional properties of the residues of the top half of the cTAR DNA (mini-cTAR) by measuring the ^{13}C relaxation properties of both aromatic and anomeric carbons. It is important to keep in mind that mini-cTAR is a model sequence that will not allow determining exactly how NC interacts with the full-length cTAR (55 nt). Indeed, the TGG motif identified as the main NC binding site in mini-cTAR is partly paired in the full-length cTAR [15,25], and thus does likely not bind NC in this sequence. Nevertheless, due to its limited size, mini-cTAR constitutes a very good model system to investigate in depth by NMR the relationships between the dynamics of DNA residues and their recognition by NC. Knowledge of the dynamics of mini-cTAR residues is important to further understand the role of the dynamics of each nucleotide in the recognition mechanism

Table 2. Internal motion parameters for mini-cTAR DNA. Due to overlapped cross-peaks and a broad peak, no models were fitted for C11, C22 sugars residues and for G14 base, respectively.

	C8/C6			C1'		
	S ²	τ _e (ps)	R _{ex} (s ⁻¹)	S ²	τ _e (ps)	R _{ex} (s ⁻¹)
C1	0.79±0.06	17.72±4.75	16.20±1.79	0.52±0.03	114.52±15.03	
C2						
A3	0.90±0.04			0.88±0.03	184.75±93.77	
G4	0.86±0.09		9.45±3.24			
A5	0.75±0.16	41.67±1.30	7.63±0.23	0.87±0.07	98.10±5.00	6.06±2.28
G6	1.00±0.04			1.00±0.03		
A7	0.86±0.03			0.80±0.06	41.22±18.29	4.61±2.21
G8	0.94±0.05		3.12±0.23	0.90±0.03	148.60±18.23	
C9	0.90±0.02			0.89±0.03		
T10	0.73±0.03	19.23±1.27				
C11	0.67±0.09	39.83±10.55	20.56±3.18	Overlap		
C12	0.81±0.05	97.23±39.86	2.23±0.12	0.87±0.03	154.30±68.57	
C13				0.77±0.02	252.22±43.34	
G14						
G15				0.88±0.03	221.76±176.86	
G16	0.95±0.04			0.89±0.03	81.65±43.45	
C17	0.88±0.03			0.83±0.03	94.32±13.23	
T18	0.91±0.03			1.00±0.03		
C19	0.88±0.03			0.95±0.03		
G20	0.89±0.04			0.76±0.05	29.40±12.31	8.43±1.74
A21	0.93±0.03					
C22	0.76±0.07	65.89±27.90	8.36±2.98	Overlap		
C23	0.84±0.03	74.84±37.68		0.79±0.03	254.73±69.54	
T24	0.73±0.03	41.43±15.99				
G25						
G26	0.84±0.03					

Other residues without values correspond to residues that do not fit any model well.
doi:10.1371/journal.pone.0038905.t002

of nucleic acids by NC and the role of the internal and apical loops on the stability of their adjacent stems. Mismatches, bulges and internal loops are regularly distributed along the TAR and cTAR hairpins delineating short double-stranded segments that can be easily melted by the weak duplex destabilizing properties of NC [2,5,6,57,58]. Moreover, the internal loop of mini-cTAR destabilizes the lower double-stranded segment [25] and favors NC binding [20] to the TGG sequence that constitutes the preferential binding site for NC(11–55) in this model sequence. In the mini-cTAR:NC(11–55), the T24 residue was found to interact with residues of the N-terminal zinc finger, while the G26 residue is inserted in the hydrophobic plateau of the C-terminal zinc finger, as in all published NC:nucleic acids complexes [11,19,21,59,60]. Using qualitative analyses of spectra and quantitative model-free analyses, we identified residues that are involved in: (i) slow motions (micro-to millisecond); (ii) fast motions (pico-to nanosecond); and (iii) the two types of motions, simultaneously. Our data are discussed in connection with our recent NMR study [20] and the gel retardation assays (Figure 2).

To gain insight into the recognition mechanism of DNA sequences by NC, it is important to understand why the G26 residue is selected in the context of mini-cTAR. Indeed, this hairpin

contains five unpaired guanines: one in the apical loop (G14 since G15 is involved in a mismatch with T10), one in the internal loop (G20) and three in the destabilized lower stem (G4, G25 and G26). Among these potential binding sites, the strong preference exhibited for a single one is puzzling. Gel retardation data (Figure 2) showed that the apical loop does not significantly bind NC(11–55). Moreover, inclusion of the 3'-end TGG sequence within a stable stem (Figures 1 and 2, mutant mini-cTARIN2) precludes strong binding of NC(11–55), showing that the 3' terminal position of G26 in mini-cTAR is not sufficient for NC(11–55) binding. This finding is consistent with data obtained with other oligonucleotides containing a guanine residue at the terminal position and that do not exhibit significant NC binding at this position [9,11,19]. For instance, the major binding site in the (-)PBS oligonucleotide is centered on a guanine located in the apical loop, whereas the guanine at the 5' terminal position is only a minor binding site [19].

Several works clearly indicated that unpaired guanines are necessary for binding NC with high affinity, and the nature of the adjacent nucleotides is important too [2,10,18,24]. Especially, the presence of a thymine at the 5' side is a favorable factor, due to direct contacts between the methyl of the thymine residue and the hydrophobic side chains of the protein [19,20]. To investigate the

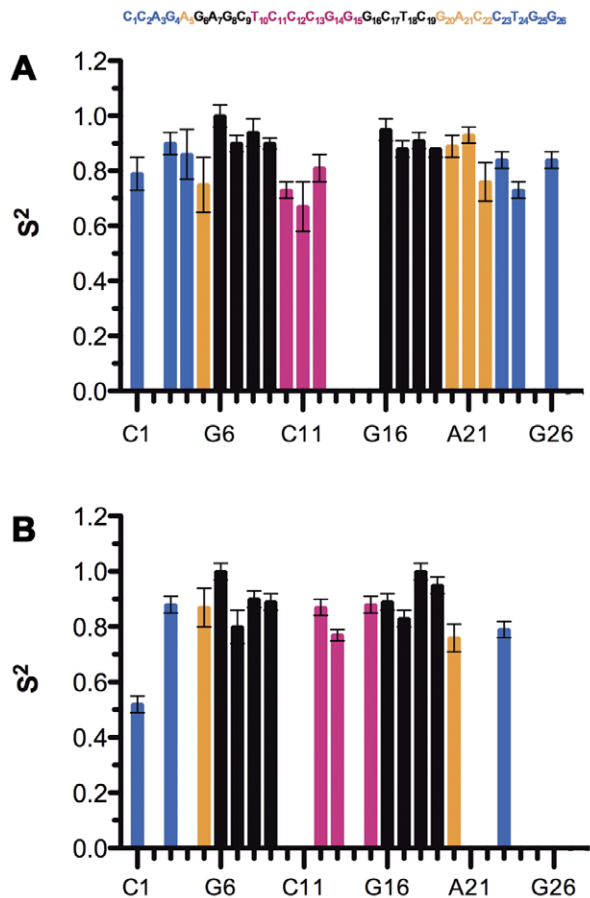


Figure 4. S^2 as extracted from model-free analysis versus sequence at 500 MHz. (A) C6/C8 spins; (B) C1' spin. Residues for which no results are shown correspond to overlapped cross-peaks or data that could not be fit well with any model-free model. The color codes used for the residues are the following: blue (lower stem), orange (internal loop), black (upper stem) and magenta (apical loop). doi:10.1371/journal.pone.0038905.g004

importance of this factor in the present case, we introduce the TGG sequence in the apical loop (Figure 1, mutants mini-cTARCT and mini-cTARIN2CT). The gel retardation experiments show a stronger binding of NC(11–55) to the mini-cTARIN2CT mutant exhibiting a TGG sequence in the apical loop, than to the mini-cTARIN2 mutant exhibiting a CGG sequence in the apical loop (Figure 2). Note that in these two mutants, the internal loop was deleted to prevent the NC binding to the TGG motif of the lower stem. Interestingly, the level of NC binding to the TGG motif is lower in the apical loop than in the lower stem (Figure 2B, compare mini-cTAR vs mini-cTAR-IN2CT). This is further supported by the data obtained with the mini-cTARCT mutant showing a moderate increase of NC binding relative to mini-cTAR, although this oligonucleotide contains two TGG sites: one in the lower stem and the other in the apical loop.

Thus, our data indicate that other factors than location of G26 at the 3'-end and the presence of a thymine at its 5' side are necessary to fully explain the selective recognition of G26 in mini-cTAR. Our previous investigations on mini-cTAR alone identified slow dynamic processes in the apical and internal loops but not in the lower stem [20]. These data prompted us to hypothesize an important role of DNA dynamics in the mechanisms of NC:DNA

recognition. To test this hypothesis, we investigated the DNA dynamics using ^{13}C NMR relaxation.

Selective Binding to NC Requires a Highly Mobile and Accessible Residue

Residues experiencing fast internal motions (low S^2) were found to be located in the apical loop (T10, C11 and C12) and in the lower stem (C1, T24 and G26). Among the G residues, the exchange contributions found for G4, G14 and G20 indicate that these residues undergo stacking or hydrogen bonding interactions with neighbor residues. In contrast, residues G6, G8 and G16 in the upper stem did not present any exchange contribution supporting their inclusion in a stable double-strand structure. Similarly, residue G15 in the apical loop did not exhibit any exchange contribution indicating that it is likely paired with the T10 residue as confirmed by the disappearance of the T10/G15 imino proton (Figure 7) when residue G15 was replaced by A15 (data not shown).

For each residue exhibiting a significant exchange contribution, we search in its neighboring a possible partner residue experiencing chemical exchange contribution in the same range of time. For the G14 residue, no conformational exchange is found for its adjacent residues C13 and G15, suggesting that these residues do not interact with G14. However, significant exchange contributions are found for residue C11 both in dispersion experiments and in spin relaxation measurements (large R_{ex} found for model 3), suggesting the existence of a transient C11–G14 base-pair (Figure 6). Interestingly, a similar cross-loop base-pair has been identified in the apical loop of TAR [52]. Noticeably, two residues separate the two partners of the C11–G14 base-pair in mini-cTAR DNA, instead of three for the apical loop of TAR RNA, suggesting that the C-G base-pair is less relaxed and stable in mini-cTAR than in TAR. Exchange contributions from dispersion relaxation measurements showed that A5 and G20 residues (Figure 6B) were involved in conformational exchange occurring in the same timescale. Therefore, a transient G.A base pair (of the shear type) likely occurs within the internal loop. This pairing, which frequently occurs in internal bulges [61], was already suggested by our structural studies [25]. Similar R_{ex} values were found for residue G4 in the lower stem and residue C22 in the internal loop indicating a possible transient pairing between these residues (Figure 6B), and thus, an alternate pairing of residue G4 with residues C22 and C23 that could explain the destabilization effect of the internal loop on the lower stem. This hypothesis is strongly supported by the analysis of the mini-cTARGC mutant (Figure 1A) that is unable to form the G4–C22 base-pair but exhibits three additional stable base-pairs in the lower stem (Figure 7). Similar base-pairs between residues of stems and internal loops have been described in the HIV-1 SL1 stem-loop [62]. Finally, residues G25 and G26 were the only G residues not involved in base-pairs (as assessed by the observation of imino protons) or in conformational exchange. Comparison of the respective dynamics of these two latter residues indicates a higher mobility of G26 relative to G25.

Taken together, our results strongly suggest that conformational exchange processes, probably associated to transient base pairing, are deleterious for NC recognition, explaining the low binding of the protein to the apical and internal loops and in contrast, its tight binding to G26 that is mobile and exempt of any pairing. In addition, we suggest that the lower binding of NC to the TGG motif in the apical loop (in mini-cTARCT and mini-cTAR-IN2CT) as compared to the TGG motif in the lower stem (mini-cTAR) is related to different dynamic processes. Of course, a full account of these effects would need a study of the dynamics of TGG inserted in the apical loop. Furthermore, it is important to

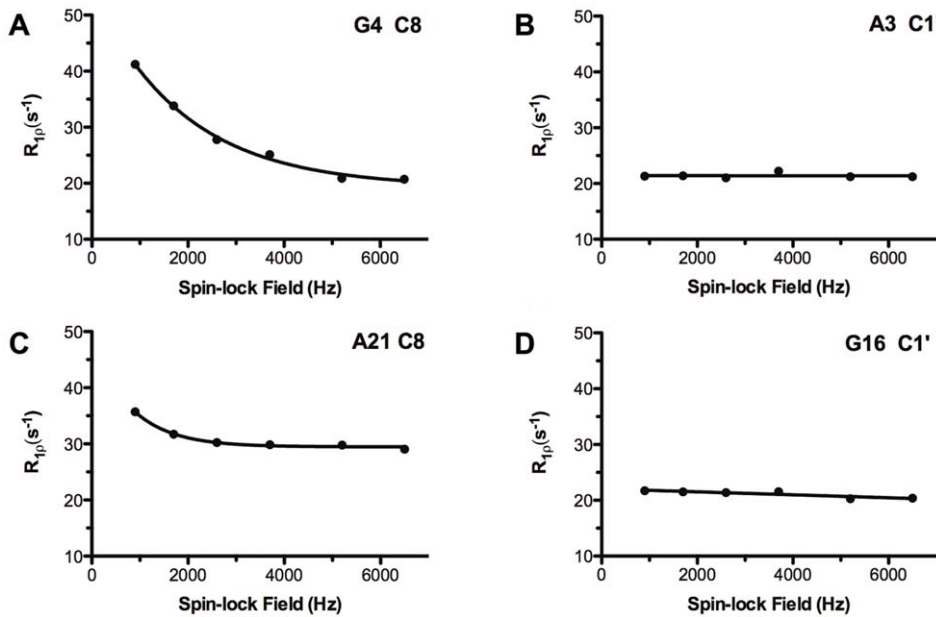


Figure 5. ¹³C transverse relaxation rates ($R_{1\rho}$) versus applied spin lock field strength (in Hertz) at 500 MHz for aromatic and anomeric carbons of mini-cTAR DNA. (A) G4 C8; (B) A3 C1'; (C) A21 C8; (D) G16 C1'. doi:10.1371/journal.pone.0038905.g005

note that the present study probes motions in two particular time-scales (the ps-ns scale from spin relaxation experiments and the μ s scale from the relaxation dispersion experiments). Therefore, we cannot rule out the possibility that intermediate ns- μ s range motions may be also important for NC binding. Exploring motions in this time range would need site-specific deuterium labeling and solid-state NMR [63,64], which are beyond the scope of the present study.

Comparisons with Data from the Literature

Taken together, our NMR and binding data support the notion that residue G26 is not involved in a stable or transient base-pair and exhibits the highest mobility and accessibility from all the guanines present in mini-cTAR. The propensity of NC to bind preferentially a highly mobile G residue is further supported by

several structural studies on oligonucleotides exhibiting a strong binding site for NC. Examination of the structures of free SL3 and SL2 [9,65] that bind NC through the GNG motif in their apical loops [11,60] shows that these guanines are totally looped out in solution in contrast to the other residues. Similarly, the structure of free PBS [19] that binds NC through the 5'-CTG-3' motif of its loop shows also that the G7 residue is partially looped out with its Watson-Crick side directed towards the solvent. Moreover, the two guanines recognized by NC in the internal loop of SL1 are also highly mobile [62]. Furthermore, a high mobility of residue G32 in the apical loop of TAR RNA was recently reported [52] and is consistent with the specific interaction of NC with the apical loop of wild-type TAR RNA [14]. In contrast, the absence of binding of NC(11-55) to the apical loop of mini-cTAR DNA could be readily explained by the low mobility and accessibility of the G residues in this loop (this work).

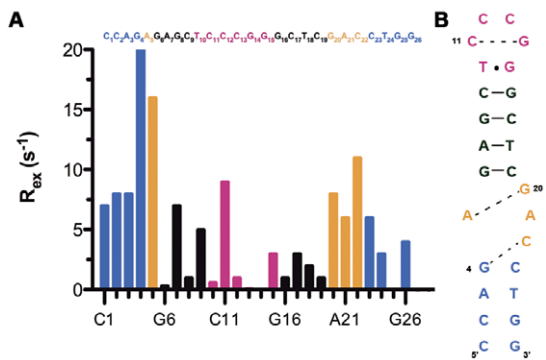


Figure 6. Exchange contribution to transverse relaxation versus sequence for aromatic C8 and C6 carbons (A) of mini-cTAR DNA determined from $T_{1\rho}$ power dependence experiments. (B) Secondary structure for the mini-cTAR sequence showing the possible transient base-pairs for G4-C22, A5-G20 and C11-G14. The color codes used for the residues are the following: blue (lower stem), orange (internal loop), black (upper stem) and magenta (apical loop). doi:10.1371/journal.pone.0038905.g006

Conclusions

The present study investigates the molecular basis of the specific binding of NC to a particular guanine in a molecule possessing five unpaired guanines [20]. The local selection appears to depend on the relative mobility and accessibility of the residues and on the presence of a thymine at the 5' side of the guanine residue. The high mobility of the G residue in the NC binding site is a direct consequence of the absence of a stable or transient base-pairing involving this residue. This is critical since the Watson-Crick side of the guanine was shown to interact with NC amino side chains and backbone atoms [11,20]. In addition, it is likely that through its high mobility, the G residue can optimally adjust to the NC hydrophobic platform at the top of the folded fingers, and notably to the Trp37 residue, whose stacking with the G residue plays a key role in the binding energy [13,66]. The key role of the oligonucleotide dynamic is also fully consistent with its role in the NC chaperone activity [67,68]. The ability of NC to discriminate between close sequences through their dynamic properties contributes to understand how the NC domain of Gag recognizes

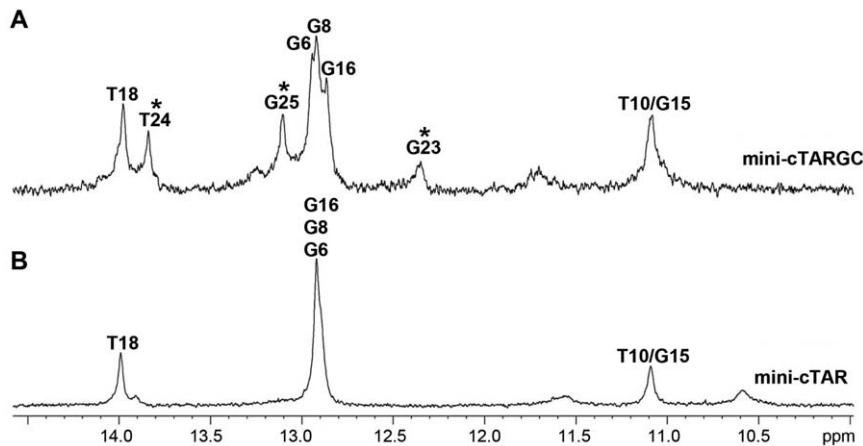


Figure 7. Imino region of 1D spectra (pH 6.5, in H₂O, 10°C, 60 ms) showing the difference between mini-cTARGC (A) and mini-cTAR (B). The new resonances observable in the mutant and corresponding to the imino protons of the lower stem are indicated by asterisks.
doi:10.1371/journal.pone.0038905.g007

the genomic RNA through specific interactions with the apical loops of SL2 and SL3.

Supporting Information

Figure S1 Representative decay curves for ¹³C relaxation experiments recorded at 500 MHz. (A) ¹³C T_1 and (B) ¹³C $T_1\rho$ experiments for: A7 C8 (black circles), G16 C8 (red triangles) and T24 C6 (blue square) resonances. The results of duplicated experiments are included to confirm the reproducibility of the data. Most decay curves could be fitted with single exponentials.
(TIF)

Figure S2 Relaxation times for anomeric C1' carbons of mini-cTAR DNA at 500 MHz. spins. Top to bottom: ¹³C T_1 , ¹³C $T_1\rho$ and hetNOEs. Errors represent uncertainties in the fit of the primary relaxation data to mono-exponential decays. No data are associated to residues corresponding to a broad or overlapped cross peak. The color codes used for the residues are the following: blue (lower stem), orange (internal loop), black (upper stem) and magenta (apical loop). **Comments of Figure 3 and Supplementary Figure S2:** The profiles of T_1 , $T_1\rho$ and hetNOE values for both C1' and C6/C8 carbons were found to be correlated with the sequence. The T_1 profile for the successive parts of the molecule could be roughly described as: low (lower stem), high (upper stem), low (apical loop), high (upper stem), high (internal loop), low (lower stem). Note that for the $T_1\rho$ and hetNOE values, the profile is reversed. This profile is more apparent when only the central part (upper stem and apical loop) is considered. The data

are therefore compatible with fast motions in the picosecond to nanosecond timescale for several residues of the apical loop. This kind of motion affects probably in an opposite way the T_1 (decrease) and $T_1\rho$ /hetNOE (increase) values [44,47]. Similar profiles for the various parameters of aromatic and C1' carbons are indicative of coupled motions for base and sugar of the various residues of mini-cTAR [47].

(TIF)

Figure S3 Region C8/C6–H8 of constant-time HSQC of ¹⁵N/¹³C labeled mini-cTAR DNA at 30°C. The cross peaks are indicated with the name of the corresponding residue. In this spectrum, G14 residue shows the broadest cross-peak among all residues of mini-cTAR (see text).
(TIF)

(TIF)

Materials S1 Description of the procedure used in Quantitative Analysis of the ¹³C relaxation data.

(DOC)

Acknowledgement

We gratefully thank Prof. G.Varani for the gift of pulse sequences for the measurement of ¹³C relaxation times.

Author Contributions

Conceived and designed the experiments: OM PF. Performed the experiments: AB LZ HDR FC. Analyzed the data: AB LZ PF BR YM OM. Wrote the paper: OM PF BR YM.

References

- Darlix JL, Godet J, Ivanyi-Nagy R, Fosse P, Mauffret O, et al. (2011) Flexible nature and specific functions of the HIV-1 nucleocapsid protein. *J Mol Biol* 410: 565–581.
- Levin JG, Guo J, Rouzina I, Musier-Forsyth K (2005) Nucleic acid chaperone activity of HIV-1 nucleocapsid protein: critical role in reverse transcription and molecular mechanism. *Prog Nucleic Acid Res Mol Biol* 80: 217–286.
- Thomas JA, Gorelick RJ (2008) Nucleocapsid protein function in early infection processes. *Virus Research* 134: 39–63.
- Darlix JL, Garrido JL, Morellet N, Mely Y, de Rocquigny H (2007) Properties, functions, and drug targeting of the multifunctional nucleocapsid protein of the human immunodeficiency virus. *Adv Pharmacol* 55: 299–346.
- Godet J, Mely Y (2010) Biophysical studies of the nucleic acid chaperone properties of the HIV-1 nucleocapsid protein. *RNA Biol* 7: 48–60.
- Levin JG, Mitra M, Mascarenhas A, Musier-Forsyth K (2010) Role of HIV-1 nucleocapsid protein in HIV-1 reverse transcription. *RNA Biol* 7.
- Mirambeau G, Lyonmais S, Gorelick RJ (2010) Features, processing states, and heterologous protein interactions in the modulation of the retroviral nucleocapsid protein function. *RNA Biol* 7: 85–95.
- Muriaux D, Darlix JL (2010) Properties and functions of the nucleocapsid protein in virus assembly. *RNA Biol* 7.
- Amarasinghe GK, De Guzman RN, Turner RB, Summers MF (2000) NMR structure of stem-loop SL2 of the HIV-1 psi RNA packaging signal reveals a novel A-U-A base-triple platform. *J Mol Biol* 299: 145–156.
- Vuilleumier C, Bombarda E, Morellet N, Gerard D, Roques BP, et al. (1999) Nucleic acid sequence discrimination by the HIV-1 nucleocapsid protein NCp7: a fluorescence study. *Biochemistry* 38: 16816–16825.
- De Guzman RN, Wu ZR, Stalling CC, Pappalardo L, Borer PN, et al. (1998) Structure of the HIV-1 nucleocapsid protein bound to the SL3 psi-RNA recognition element. *Science* 279: 384–388.

12. Lapadat-Tapolsky M, De Rocquigny H, Van Gent D, Roques B, Plasterk R, et al. (1993) Interactions between HIV-1 nucleocapsid protein and viral DNA may have important functions in the viral life cycle. *Nucleic Acids Res* 21: 831–839.
13. Beltz H, Clauss C, Piemont E, Ficheux D, Gorelick RJ, et al. (2005) Structural determinants of HIV-1 nucleocapsid protein for cTAR DNA binding and destabilization, and correlation with inhibition of self-primed DNA synthesis. *J Mol Biol* 348: 1113–1126.
14. Kanevsky I, Chaminade F, Ficheux D, Moumen A, Gorelick R, et al. (2005) Specific interactions between HIV-1 nucleocapsid protein and the TAR element. *J Mol Biol* 348: 1059–1077.
15. Kanevsky I, Chaminade F, Chen Y, Godet J, Rene B, et al. (2011) Structural determinants of TAR RNA-DNA annealing in the absence and presence of HIV-1 nucleocapsid protein. *Nucleic Acids Res* 39: 8148–8162.
16. Wang H, Yeh YS, Barbara PF (2009) HIV-1 nucleocapsid protein binds double-stranded nucleic acids. *J Am Chem Soc* 131: 15534–15543.
17. Avilov SV, Godet J, Piemont E, Mely Y (2009) Site-specific characterization of HIV-1 nucleocapsid protein binding to oligonucleotides with two binding sites. *Biochemistry* 48: 2422–2430.
18. Fisher RJ, Rein A, Fivash M, Urbaneja MA, Casas-Finet JR, et al. (1998) Sequence-specific binding of human immunodeficiency virus type 1 nucleocapsid protein to short oligonucleotides. *J Virol* 72: 1902–1909.
19. Bourbigot S, Ramalanjaona N, Boudier C, Salgado GF, Roques BP, et al. (2008) How the HIV-1 nucleocapsid protein binds and destabilises the (−)primer binding site during reverse transcription. *J Mol Biol* 383: 1112–1128.
20. Bazzi A, Zargarian L, Chaminade F, Boudier C, De Rocquigny H, et al. (2011) Structural insights into the cTAR DNA recognition by the HIV-1 nucleocapsid protein: role of sugar deoxyriboses in the binding polarity of NC. *Nucleic Acids Res*.
21. Morellet N, Demene H, Teilleux V, Huynh-Dinh T, de Rocquigny H, et al. (1998) Structure of the complex between the HIV-1 nucleocapsid protein NCp7 and the single-stranded pentanucleotide d(ACGCC). *J Mol Biol* 283: 419–434.
22. Lu K, Heng X, Summers MF (2011) Structural Determinants and Mechanism of HIV-1 Genome Packaging. *J Mol Biol* 410: 609–633.
23. Watts JM, Dang KK, Gorelick RJ, Leonard CW, Bess JW, Jr., et al. (2009) Architecture and secondary structure of an entire HIV-1 RNA genome. *Nature* 460: 711–716.
24. Gherghe C, Lombo T, Leonard CW, Datta SA, Bess JW, Jr., et al. (2010) Definition of a high-affinity Gag recognition structure mediating packaging of a retroviral RNA genome. *Proc Natl Acad Sci U S A* 107: 19248–19253.
25. Zargarian L, Kanevsky I, Bazzi A, Boynard J, Chaminade F, et al. (2009) Structural and dynamic characterization of the upper part of the HIV-1 cTAR DNA hairpin. *Nucleic Acids Res* 37: 4043–4054.
26. Godet J, de Rocquigny H, Raja C, Glasser N, Ficheux D, et al. (2006) During the early phase of HIV-1 DNA synthesis, nucleocapsid protein directs hybridization of the TAR complementary sequences via the ends of their double-stranded stem. *J Mol Biol* 356: 1180–1192.
27. Vo MN, Barany G, Rouzina I, Musier-Forsyth K (2006) Mechanistic studies of mini-TAR RNA/DNA annealing in the absence and presence of HIV-1 nucleocapsid protein. *J Mol Biol* 363: 244–261.
28. Vo MN, Barany G, Rouzina I, Musier-Forsyth K (2009) Effect of Mg²⁺ and Na⁺ on the nucleic acid chaperone activity of HIV-1 nucleocapsid protein: implications for reverse transcription. *J Mol Biol* 386: 773–788.
29. Basu VP, Song M, Gao L, Rigby ST, Hanson MN, et al. (2008) Strand transfer events during HIV-1 reverse transcription. *Virus Res* 134: 19–38.
30. Al-Hashimi HM, Gosser Y, Gorin A, Hu W, Majumdar A, et al. (2002) Concerted motions in HIV-1 TAR RNA may allow access to bound state conformations: RNA dynamics from NMR residual dipolar couplings. *J Mol Biol* 315: 95–102.
31. Aboulela F, Karn J, Varani G (1995) The Structure of the Human-Immunodeficiency-Virus Type-1 Tar Rna Reveals Principles of Rna Recognition by Tat Protein. *J Mol Biol* 253: 313–332.
32. Puglisi JD, Tan RY, Calnan BJ, Frankel AD, Williamson JR (1992) Conformation of the Tar Rna-Arginine Complex by Nmr-Spectroscopy. *Science* 257: 76–80.
33. Zhang Q, Sun X, Watt ED, Al-Hashimi HM (2006) Resolving the motional modes that code for RNA adaptation. *Science* 311: 653–656.
34. Zhang Q, Stelzer AC, Fisher CK, Al-Hashimi HM (2007) Visualizing spatially correlated dynamics that directs RNA conformational transitions. *Nature* 450: 1263–1267.
35. Bothe JR, Nikolova EN, Eichhorn CD, Chugh J, Hansen AL, et al. (2011) Characterizing RNA dynamics at atomic resolution using solution-state NMR spectroscopy. *Nat Methods* 8: 919–931.
36. Mittermaier A, Kay LE (2006) New tools provide new insights in NMR studies of protein dynamics. *Science* 312: 224–228.
37. Mittermaier AK, Kay LE (2009) Observing biological dynamics at atomic resolution using NMR. *Trends Biochem Sci* 34: 601–611.
38. Palmer AG, 3rd, Kroenke CD, Loria JP (2001) Nuclear magnetic resonance methods for quantifying microsecond-to-millisecond motions in biological macromolecules. *Methods Enzymol* 339: 204–238.
39. Palmer AG, 3rd, Massi F (2006) Characterization of the dynamics of biomacromolecules using rotating-frame spin relaxation NMR spectroscopy. *Chem Rev* 106: 1700–1719.
40. Shvadchak VV, Klymchenko AS, de Rocquigny H, Mely Y (2009) Sensing peptide-oligonucleotide interactions by a two-color fluorescence label: application to the HIV-1 nucleocapsid protein. *Nucleic Acids Res* 37: e25.
41. Boisbouvier J, Wu Z, Ono A, Kainosho M, Bax A (2003) Rotational diffusion tensor of nucleic acids from 13C NMR relaxation. *J Biomol NMR* 27: 133–142.
42. Duchardt E, Schwalbe H (2005) Residue specific ribose and nucleobase dynamics of the cUUCGg RNA tetraloop motif by MNMR 13C relaxation. *J Biomol NMR* 32: 295–308.
43. Ying JF, Grishaev A, Bryce DL, Bax A (2006) Chemical shift tensors of protonated base carbons in helical RNA and DNA from NMR relaxation and liquid crystal measurements. *Journal of the American Chemical Society* 128: 11443–11454.
44. Shajani Z, Varani G (2008) 13C relaxation studies of the DNA target sequence for hhai methyltransferase reveal unique motional properties. *Biochemistry* 47: 7617–7625.
45. Bryce DL, Grishaev A, Bax A (2005) Measurement of ribose carbon chemical shift tensors for A-form RNA by liquid crystal NMR spectroscopy. *Journal of the American Chemical Society* 127: 7387–7396.
46. Mandel AM, Akke M, Palmer AG, 3rd (1995) Backbone dynamics of Escherichia coli ribonuclease HI: correlations with structure and function in an active enzyme. *J Mol Biol* 246: 144–163.
47. Shajani Z, Varani G (2005) 13C NMR relaxation studies of RNA base and ribose nuclei reveal a complex pattern of motions in the RNA binding site for human U1A protein. *J Mol Biol* 349: 699–715.
48. Yamazaki T, Muhandiram R, Kay LE (1994) Nmr Experiments for the Measurement of Carbon Relaxation Properties in Highly Enriched, Uniformly C-13,N-15-Labeled Proteins - Application to C-13(Alpha) Carbons. *Journal of the American Chemical Society* 116: 8266–8278.
49. Bryce DL, Grishaev A, Bax A (2005) Measurement of ribose carbon chemical shift tensors for A-form RNA by liquid crystal NMR spectroscopy. *J Am Chem Soc* 127: 7387–7396.
50. Ying J, Grishaev A, Bryce DL, Bax A (2006) Chemical shift tensors of protonated base carbons in helical RNA and DNA from NMR relaxation and liquid crystal measurements. *J Am Chem Soc* 128: 11443–11454.
51. Oberstrass FC, Allain FH, Ravindranathan S (2008) Changes in dynamics of SRE-RNA on binding to the VTS1p-SAM domain studied by 13C NMR relaxation. *J Am Chem Soc* 130: 12007–12020.
52. Dethoff EA, Hansen AL, Musselman C, Watt ED, Andricioaei I, et al. (2008) Characterizing complex dynamics in the transactivation response element apical loop and motional correlations with the bulge by NMR, molecular dynamics, and mutagenesis. *Biophys J* 95: 3906–3915.
53. Tjandra N, Feller SE, Pastor RW, Bax A (1995) Rotational diffusion anisotropy of human ubiquitin from N-15 NMR relaxation. *Journal of the American Chemical Society* 117: 12562–12566.
54. Hansen AL, Al-Hashimi HM (2007) Dynamics of large elongated RNA by NMR carbon relaxation. *J Am Chem Soc* 129: 16072–16082.
55. Rule GS, Hitchens T.K. (2006) *Fundamentals of Protein NMR Spectroscopy*. Netherlands: Springer.
56. Palmer RF, Blanchard S, Jean CR, Mandell DS (2005) School district resources and identification of children with autistic disorder. *Am J Public Health* 95: 125–130.
57. Beltz H, Azoulay J, Bernacchi S, Clamme JP, Ficheux D, et al. (2003) Impact of the terminal bulges of HIV-1 cTAR DNA on its stability and the destabilizing activity of the nucleocapsid protein NCp7. *J Mol Biol* 328: 95–108.
58. Beltz H, Piemont E, Schaub E, Ficheux D, Roques B, et al. (2004) Role of the structure of the top half of HIV-1 cTAR DNA on the nucleic acid destabilizing activity of the nucleocapsid protein NCp7. *J Mol Biol* 338: 711–723.
59. Spriggs S, Garyu L, Connor R, Summers MF (2008) Potential intra- and intermolecular interactions involving the unique-5' region of the HIV-1 5'-UTR. *Biochemistry* 47: 13064–13073.
60. Amarasinghe GK, De Guzman RN, Turner RB, Chancellor KJ, Wu ZR, et al. (2000) NMR structure of the HIV-1 nucleocapsid protein bound to stem-loop SL2 of the psi-RNA packaging signal. Implications for genome recognition. *J Mol Biol* 301: 491–511.
61. Schroeder SJ, Turner DH (2000) Factors affecting the thermodynamic stability of small asymmetric internal loops in RNA. *Biochemistry* 39: 9257–9274.
62. Sun X, Zhang Q, Al-Hashimi HM (2007) Resolving fast and slow motions in the internal loop containing stem-loop 1 of HIV-1 that are modulated by Mg²⁺ binding: role in the kissing-duplex structural transition. *Nucleic Acids Res* 35: 1698–1713.
63. Olsen GL, Echodu DC, Shajani Z, Bardaro MF, Varani G, et al. (2008) Solid-state deuterium NMR studies reveal mu s-n motions in the HIV-1 Transactivation response RNA recognition site. *Journal of the American Chemical Society* 130: 2896–2897.
64. Olsen GL, Bardaro MF, Echodu DC, Drobny GP, Varani G (2010) Intermediate Rate Atomic Trajectories of RNA by Solid-State NMR Spectroscopy. *Journal of the American Chemical Society* 132: 303–308.
65. Pappalardo L, Kerwood DJ, Pelczer I, Borer PN (1998) Three-dimensional folding of an RNA hairpin required for packaging HIV-1. *J Mol Biol* 282: 801–818.
66. Mely Y, Piemont E, Sorinas-Jimeno M, de Rocquigny H, Jullian N, et al. (1993) Structural and dynamic characterization of the aromatic amino acids of the human immunodeficiency virus type I nucleocapsid protein zinc fingers and

- their involvement in heterologous tRNA(Phe) binding: a steady-state and time-resolved fluorescence study. *Biophys J* 65: 1513–1522.
67. Avilov SV, Piemont E, Shvadchak V, de Rocquigny H, Mely Y (2008) Probing dynamics of HIV-1 nucleocapsid protein/target hexanucleotide complexes by 2-aminopurine. *Nucleic Acids Res* 36: 885–896.
68. Godet J, Ramalanjaona N, Sharma KK, Richert L, de Rocquigny H, et al. (2011) Specific implications of the HIV-1 nucleocapsid zinc fingers in the annealing of the primer binding site complementary sequences during the obligatory plus strand transfer. *Nucleic Acids Res* 39: 6633–6645.